Journal of Electronic Materials
https://doi.org/10.1007/s11664-021-09396-4

ORIGINAL RESEARCH ARTICLE

Aerosol Jet Printing of SU-8 as a Passivation Layer Against Ionic Solutions

Shulin Ye[1] · **Nicholas X Williams**[1] · **Aaron D. Franklin**[1]

Received: 18 August 2021 / Accepted: 13 December 2021

Abstract

To ensure stability for low-cost electronics used in direct contact with ionic solutions (such as electronic biosensors), electrodes are frequently passivated to protect against current leakage, which leads to corrosion. The epoxy-based polymer SU-8 yields favorable properties for passivation against ionic solutions. However, it is nearly universally patterned via cleanroom techniques, which increases device cost and fabrication complexity. Printing electronic components has been shown to be a viable approach for decreasing fabrication cost. Previous reports on SU-8 printing focus on the resultant printed structure, with little emphasis on its subsequent use as a passivation layer. Here, we demonstrate the printing of SU-8 with an aerosol jet printer using ultrasonic aerosolization. We show that SU-8 can be printed without reformulation, and that printed SU-8 is a viable passivation layer over conductive silver lines, when tested in ionic solutions. Extending the printed SU-8 film beyond the underlying conductive electrodes by 100 µm produced a decrease in leakage current by six orders of magnitude and resulted in high stability over 20 voltage sweeps. Finally, we optimized the post-printing cure time to 15 min at 160°C, which further minimized leakage current. While the development of low-cost, electronic biosensing devices has increasingly moved towards printing methods, the lack of a printed passivation strategy has hindered this transition. The advancements made in this study towards an aerosol jet printable SU-8 passivation layer provide useful progress towards a fully printed, stable electronic biosensing device.

Graphical Abstract

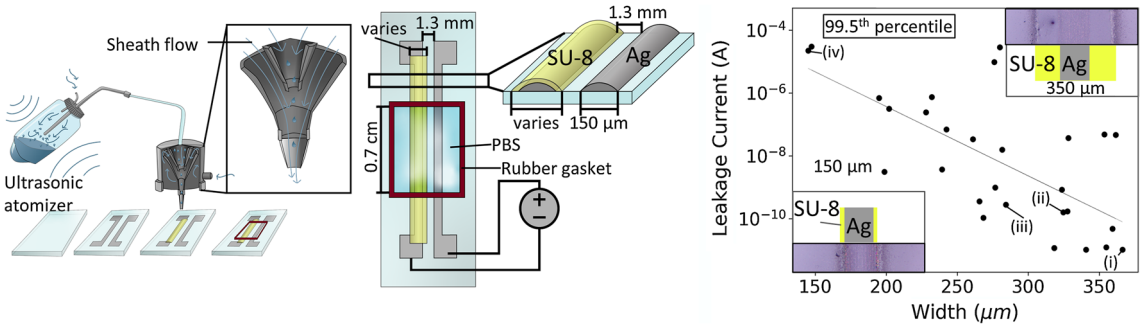

Keywords Aerosol jet printing · SU-8 · passivation · direct write · encapsulation

Introduction

Point-of-care (POC) sensors allow for more detailed monitoring of medical conditions as they enable at-home and patient-guided measurement of biological signals, facilitating a growing market that is expected to be a $27.4 billion industry by 2022.[1] Compared to traditional laboratory tests,

✉ Aaron D. Franklin
aaron.franklin@duke.edu

[1] Department of Electrical and Computer Engineering, Duke University, Durham, NC 27708, USA

Published online: 18 January 2022

POC tests eliminate lab turnaround time and enable more data-informed, patient-guided therapies.[2] Electrically transduced biosensors show promise as POC devices due to their high sensitivity, low cost, ease of use, and no requirement for analyte labeling.[3] There are two main types of electrically transduced biosensors: impedance-based and transistor-based. Both use biological recognition elements (such as an antibody or aptamer) and parlay the high transconductance of electrical components to make very sensitive biosensors. Impedance-based biosensors consist of an exposed electrode and measure change in impedance caused by the analyte binding to the biological recognition element,[4] while transistor-based biosensors use analyte binding to gate the semiconducting channel of the transistor.[5] In both of these cases, electrical elements exposed to biological fluids often show drift in their electrical properties over time.[6] In addition, electrochemical reactions can cause corrosion and bubble formation,[7] degrading sensor performance over time.[8] As most biosensors are tested by spiking in analytes in intervals, any drift in outputs during the spiking-in process complicates analysis and may cause inaccurate results.

To mitigate this drift in measured electrical response, electrically transduced biosensors are traditionally passivated, both to reduce leakage current from solution to the electrodes and to protect the sensors from the ions in the solution. Common passivation materials include compounds such as silicon nitride,[9] silicon dioxide,[9] and others[7,10]; and polymers such as PMMA[11,12] polyimide,[13] parylene,[14] and SU-8.[15–17] Some combine both materials, theorizing that polymers and oxides block different pathways.[13,18] While oxides are more commonly used as dielectrics for transistors and thus CMOS-based biosensors,[6] polymers allow for easy patterning, are generally considered better at excluding ions from solution,[13] and are commonly used in thin-film transistors, as they are compatible with printing.[19]

First formulated as a negative photoresist, SU-8 has become a common passivation layer for electrical biosensors,[15–17,20] due to its low cost[21] and biocompatibility.[22] Named because it contains (on average) 8 epoxy groups per monomer, it forms a densely cross-linked network upon exposure to UV light that is resistant to chemical etching and degradation from mechanical stress, making it an ideal passivation layer for a low-cost and flexible biosensor.[23] While SU-8 has frequently been used in microelectromechanical systems (MEMS)[21] and microfluidics,[24] it is traditionally patterned via photolithography, which requires expensive photomasks and a cleanroom process, divorcing the cost of the final product from the materials cost of the SU-8 and increasing processing complexity.[25]

Printing, specifically direct-write techniques such as inkjet and aerosol jet printing, has recently drawn considerable attention as a lower-cost alternative to cleanroom methods, especially for large-area devices such as thin-film transistors.[26] For disposable biosensors, which require very low costs to be economically feasible,[25] printing all layers, including the passivation layer, is especially favored as it has been demonstrated to adequately deposit each layer of a biosensor, including the fragile antibodies often used as detection elements,[27] which may reduce fabrication complexity and cost. Aerosol jet printers, in particular, have drawn attention due to their ability to print smaller feature sizes than inkjet printers and a wider array of inks[28] without incidences of nozzle clogs.[29] Using ultrasonic energy, the atomizer drives the ink into a dense aerosol mist,[30] and an inert gas sheath flow helps direct the mist out of the nozzle and towards the substrate. Aerosol jet printing has been used in a variety of applications, including sensors for pressure,[31] prothrombin time,[32] pH,[33] and immunoassays.[34] SU-8 6000.5 has a viscosity of 2.5 cp,[35] making it easily printable with an aerosol jet printer. SU-8 has been successfully printed with both inkjet printers[36–38] and aerosol jet printers[39]; however, in each of these previous experiments, only SU-8's resultant structural properties were analyzed. Little emphasis has been placed on the ability of printed SU-8 to passivate electrical components. Additionally, for the previous aerosol jet study, the SU-8 was reformulated to make it printable.

In this study, SU-8 was printed, without reformulation, using an aerosol jet printer with ultrasonic atomization. We show that printed SU-8 can act as a passivation layer, yielding leakage currents of less than 100 pA, with the quality of the passivation being dependent on the width of printed SU-8 covering conducting electrodes. As very few papers report the long-term stability of their sensors,[40] and because we believe that stability of the passivation layer may affect sensor stability, we analyzed the long-term (hours) stability of printed SU-8 and discovered that the film does not degrade significantly over time. Finally, we optimized hard-bake times for passivation against ionic solutions and found that an extended hard-bake time of 15 min minimized leakage current. We anticipate that this process can be used to help create fully printed biosensors, as the printing of this passivation layer had previously not been studied.

Materials and Methods

Materials

Two different brands of silver nanoparticles (AgNP) were used for this study. NovaCentrix Metalon JS-A221AE, a water-based silver ink, was used without alternation. UT Dots (UTDAg40X-30 mL), a xylene-based silver ink, was mixed 9:1 (v/v) with α-terpinol to suppress the coffee-ring effect and reduce overspray. SU-8 TF 6000.5 was acquired from Sigma-Aldrich and was kept in an amber room to avoid being accidentally exposed to UV light. Cyclopentanone

(Beantown Chemical, >99%) was used to dilute the SU-8, as it is a solvent already present in the SU-8 (alongside gamma-butyrolactone).

Substrate Preparation

Glass slides were used as substrates for each experiment. Before printing the first layer, slides were sonicated for at least 5 min in acetone before being rinsed with deionized (DI) water and dried with nitrogen.

Aerosol Jet Printing

All printing was done with an Optomec Aerosol Jet Printer (AJ-300) with a 150 μm nozzle. For each ink, the glass vial was filled with 1 mL of ink and kept at a consistent temperature via a water bath.

- *SU-8* Ink was kept at a constant temperature of 45°C to enable atomization, and the printer platen was left at room temperature, as preliminary tests showed that platen temperature was irrelevant. The ultrasonic atomizer was set to 420 mA. As rectangles in aerosol jet printing are created by printing many lines spaced closely together, the line spacing is a useful parameter because it influences how much ink is placed down. The line spacing used for the SU-8 is 50 μm (details in supplementary Fig. S1). To find good printing parameters, single lines and rectangles were printed at differing sheath flows, atomizer flows, and print speeds. After starting the sheath flow, we waited at least 5 min to allow coherent lines to form. Prints were sufficiently fast (≈2 min) that process drift should not have been a problem. After initial testing, we settled on a sheath flow of 20 sccm, an atomizer flow of 20 sccm, and a processing speed of 7 mm/s. Next, the SU-8 was soft-baked at 65°C for 2 min and 95°C for 5 min and exposed to UV light ($\lambda = 365$ nm) for 30 s at 1500 mJ/cm^2. Finally, the SU-8 was hard-baked at 160°C for 1 h (apart from the third set of experiments, where the hard-bake time varied).
- *NovaCentrix AgNP* A sheath flow rate of 20 sccm, atomizer flow rate of 20 sccm, ultrasonic atomizer current of 350-360 μA, and a processing speed of 8 mm/s were used to print traces of width approximately 150 μm with a line spacing of 15 μm. Ink was kept at 20°C, and the platen was left at room temperature. Traces were then sintered at 200°C for 1 h to yield conductive traces.
- *UT Dots AgNP* Similar to the NovaCentrix ink, silver traces of width approximately 150 μm with a line spacing of 15 μm were printed. A sheath flow rate of 25 sccm, atomizer flow rate of 20 sccm, ultrasonic atomizer current of 420 μA, and a processing speed of 7 mm/s were used. Ink was kept at 20°C, but the platen was raised to 60°C. Afterwards, the traces were sintered at 200°C for 1 h to make them conductive.

Imaging

All pictures were taken with a Zeiss AxioLab A1.

Initial Tests

Glass slides were cleaned as listed above, and SU-8 was then printed using the above parameters and imaged.

Width-Dependent Leakage Test Chip Fabrication

Glass slides used as substrates were cleaned as above. NovaCentrix AgNP traces were printed as above. The traces were approximately 150 μm wide as determined by optical microscopy, more than 0.7 cm long, and were spaced 1.3 mm apart. Lines were checked for conductivity using a source-measure unit and non-conductive lines were rejected.

For this experiment, a 1:1 (v/v) mix of SU-8 and cyclopentanone was used and printed with parameters as above. The width of the SU-8 varied from being equal or slightly narrower than the underlying silver to extending 100 μm on each side. Slides were visually inspected and samples with visible holes in the SU-8 layer were rejected.

Hard-Bake Time Test Chips

Glass slides, used as substrates, were cleaned as above. UT Dots AgNP traces were printed as above, to the same dimensions as in the previous experiment. Lines were checked for conductivity and non-conductive lines were rejected.

Next, a layer of the adhesion promoter, P20, was spun atop the samples. Undiluted SU-8 was used in this experiment and was printed using the same parameters as above. The final width of SU-8 was approximately 350 μm. Finally, the slides were hard-baked for various lengths of time. Samples with visible holes in the SU-8 layer were removed from analysis.

Electrical Measurements in Ionic Solutions

A rubber gasket (0.7 cm on each side) was placed over each sample and filled with 100 μL of phosphate-buffered saline (PBS). Figure 2 a shows a diagram of the printed pattern and the testing setup. All electrical measurements were taken with a Keysight B2902A Precision Source/Measure Unit using a Signatone probe station. To avoid the silver delaminating, voltage was limited to between − 0.5V and 0.5V. The voltage between the two printed silver lines was swept from − 0.5 V to 0.5 V and then back from 0.5 V to − 0.5 V, with 1000 data points for each direction, while the leakage

current between the two lines was measured. Each sweep took about 2 min.

Results and Discussion

SU-8 Ink Development and Printing Parameters

The SU-8 was first optimized for aerosol jet printing. Aerosol jet printing is a direct-write fabrication technique that uses an inert nitrogen gas atomizer flow to propel aerosolized ink (Fig. 1a) from the ink vial to the printer head (Fig. 1b) for deposition directly onto a substrate as guided by a computer-aided design (CAD) file that directs the x-y motor that controls the location of the printer head. While this method allows for printing of inks with a much wider viscosity range as compared to inkjet printing,[28] multiple parameters must be tuned to enable printing of SU-8, which is a relatively low-viscosity ink, into coherent shapes. The positive pressure of the atomizer gas flow that guides the ink towards the surface must be balanced against the negative pressure of the sheath flow, which concentrates the ink towards the substrate surface and prohibits any contact between ink and nozzle side walls, prolonging possible printing times considerably as compared to inkjet printing.[41]

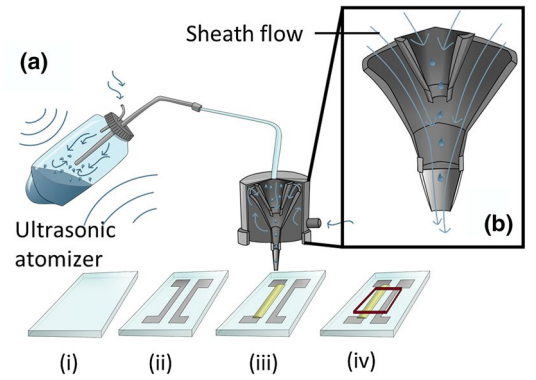

(c) Printer parameters (sccm)

SH	20	20	20	30
ATM	10	15	20	25

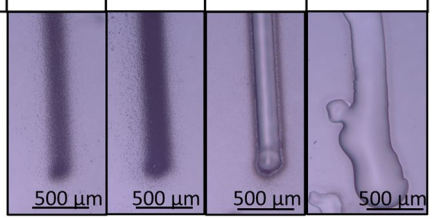

Fig. 1 Aerosol jet printing of SU-8. (a) Diagram of aerosol jet printing used in this work, including process flow: (i) glass slides were cleaned with acetone; (ii) silver nanoparticles were printed into traces and sintered at 200°C for 1 h; (iii) SU-8 was printed to cover silver traces, soft-baked, exposed to UV light, and hard-baked; and (iv) a rubber gasket was placed over the lines and filled with PBS for testing. (b) Illustration of how the protective sheath flow focuses the aerosol jet and reduces clogging during printing. (c) Undiluted SU-8 TF 6000.5 can be printed, after adjusting sheath (SH) and atomizer (ATM) flows, into well-defined lines. All flow rates are given in standard cubic centimeters per minute (sccm).

Undiluted SU-8 TF 6000.5 can be directly printed with an aerosol jet printer forming neat lines with well-defined borders (Fig. 1c). Previous papers have started with more viscous formulations of SU-8, requiring them to dilute the SU-8 before printing. For example, Bernasconi et al. tested tetrahydrofuran, *N*-methyl-2-pyrrolidone, and cyclopentanone as possible solvents to dilute SU-8 2005 for inkjet printing.[38] Eckstein et al. diluted SU-8 2025 in γ-butyrolactone and 3-heptanone to achieve a printable mixture.[39] Removing the dilution step simplifies the ink preparation, and diluting the ink may affect the polymerization process and resultant performance as a passivation layer. However, diluting the ink may improve line quality, so there are trade-offs to be made.

When deposition rates are insufficient, the aerosol jet print consists of only small errant droplets called overspray,[28] instead of forming a uniform film (Fig. 1c). If the flow rates are too high, too much ink is printed down before solvent evaporation, and the printed ink forms uneven bulges. It was found that a sheath flow of 20 sccm and an atomizer flow of 20 sccm produced a coherent line that had little overspray. The line width achieved is comparable to what was previously reported by Eckstein et al., who reported lines of approximately 60 µm width[39]; by properly controlling the printing speed we achieved line widths down to ≈60 µm while still maintaining a coherent deposition with limited overspray (supplementary Fig. S2).

While modifying the printer flow rates yielded some decrease in overspray, we investigated other methods to further decrease the arrant droplet deposition, and thus improve edge definition. Thinning the SU-8 with cyclopentanone (a solvent already present in the SU-8) was found to further reduce overspray, as seen in supplementary Fig. S3. Evaluation of dilutions from 10-100% revealed that an equal amount of cyclopentanone and SU-8 (v/v) minimizes the overspray while maintaining line integrity.

In addition to overspray, pinholes, especially near the edge, are a known issue for printed polymers when they are utilized as electrical insulators.[26] While excessive pinholing was not observed for the majority of our printed SU-8 traces, about 21% of our slides did have visible edge defects, and we removed these from further analysis. Further optimization is needed to eliminate pinholes from printed SU-8 passivation layers, which may be achieved through further optimization of the printing conditions or ink formulation.

Width-Dependent Passivation

Next, we analyzed the ability of printed SU-8 to passivate electronic devices in ionic solutions. Traditionally, the thickness of the dielectric layer is the defining factor determining the efficacy of the passivation; however, as can be seen in Fig. 1c, additional deposition of the SU-8 does not increase the thickness of the print, merely the deposited width. To investigate the width-dependent passivation, we printed two traces of silver and covered one with SU-8 (Fig. 2a). To take electrical measurements, a rubber gasket (0.7 cm on each side) was placed over each sample and filled with 100 µL of PBS (Fig. 2a). Using a source-measure unit (SMU), which both applies a voltage and measures the current, the voltage between the two printed silver traces was swept from −0.5V to 0.5V, and the resulting leakage current was measured. The leakage current was measured against the printed width of the SU-8 (i.e., the extent which the SU-8 covers the conductive electrodes). We chose to measure the total width of the SU-8 instead of the extension from each side because measuring the extension from the silver line is more error-prone due to the overspray from the silver, and because the width is what can be controlled more precisely than the extension (see inset images of Fig. 2d and e for examples). Additionally, width was investigated because thickness is a difficult parameter to control in a singular formulation of SU-8, given that added layers will redissolve previously printed, uncured layers. While curing each layer without removing the substrate from the printer is possible,[38] it would complicate fabrication and risk clogs.

There is an inverse and log-linear correlation between leakage current and the printed width of the SU-8 passivation layer (Fig. 2c), with a small number of samples having widths greater than 300 µm measured at the lowest value the SMU could record (10^{-11} A). Given that the exposed area for each trace is approximately 0.0105 cm^2, standardizing the leakage current for the exposed electrode area yields a leakage current of approximately 0.95 nA per cm^2. Initially, we looked at the highest absolute value of the current across the voltage sweep range instead of simply measuring at a specific voltage. However, as some datasets have extreme outliers (supplementary Fig. S4), we chose to look at the 99.5th percentile to exclude these peaks, which we attribute to noise from the high measurement frequency utilized.

Each sweep test was performed 20 times to investigate the stability of the SU-8 (Fig. 2f). At very low leakage levels (10 pA with a width of 365 µm-as shown in Fig. 2d), the current is linear. For cases where the leakage current is higher, some curvature is visible, indicating more electrochemical reactions. At slightly higher leakage levels [Fig. 2f(ii)], increased noise is observed in the curve, which may indicate the movement of ions.[13] At the thinnest widths, where the SU-8 is approximately the same width as the silver (150 µm, Fig. 2e), the maximum leakage current hits the compliance current of the SMU (100 µA). The current peaks around ± 0.1 V, showing that the current is dominated by electrochemical reactions. While the leakage current increases after each sweep, the passivation does not degrade significantly after 20 sweeps (supplementary Fig. S5a). More than 2/3 of samples do not degrade more than 25-fold, although a few show hundred-fold degradation (supplementary Fig. S5b). Further investigation is required to understand the cause of the significant increase in leakage current over time for the small minority of samples. A stable reading over time is a pivotal aspect of biosensors, as measurement of a specific analyte is typically dependent on a deviation from a baseline.

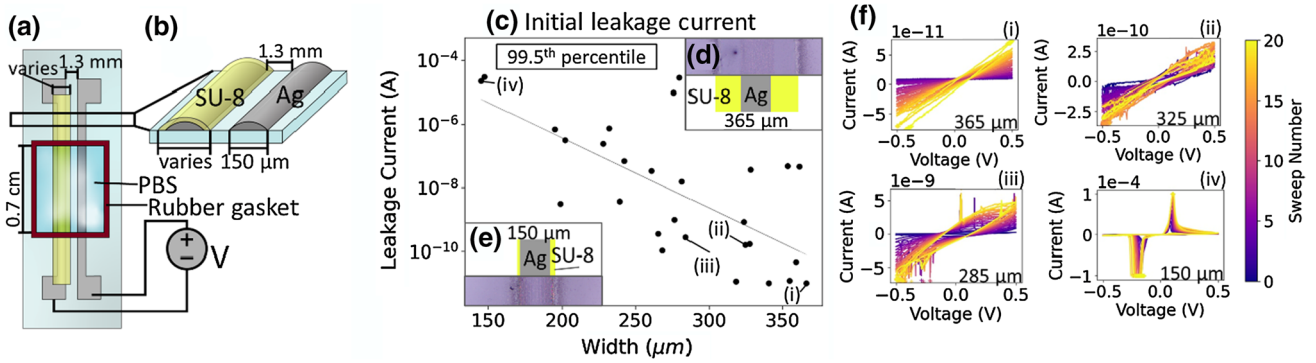

Fig. 2 Width dependence of printed SU-8 passivation. (a) Schematic of leakage testing setup. A rubber gasket is used to encapsulate the testing area and is filled with 100 µL of PBS. Voltage was applied between the two silver leads and swept from −0.5 V to 0.5 V and back again. (b) Cross-sectional illustration showing SU-8 (yellow) coverage of printed Ag electrode (depicted in grey), with the variable SU-8 width indicated. (c) Initial leakage current (99.5th percentile) declines as the width of SU-8 increases. Insets: Top-view images showing examples of (d) 350 µm and (e) 150 µm wide SU-8 with aligned schematics showing the exact width and location and width of the printed Ag line in grey and the location and width of the SU08 passivation layer in yellow. (f) 20 sweep passes for indicated data points in (c), showing increased leakage over time (i.e., sweep number).

If the baseline measurement drifts over time, it may be more difficult (or impossible) to obtain a quantitative measurement of the exact concentration of an analyte, either leading to a spurious measurement or relegating a device with a high temporal drift to qualitative measurements. Unfortunately, long-term degradation studies and temporal performance drift of passivation layers are typically not performed in the literature, making the information provided in these results of important insight to the field.

Unfortunately, while SU-8 is a commonly used passivation layer, little direct investigation has been performed on its ability to passivate. Other photoresists are sometimes used to passivate, and some have also been printed for structural purposes[42] and as the dielectric layer in capacitors,[43] but we were unable to identify studies showing other photoresists printed as passivation layers. Hammond et al. show a leakage current of less than 120 pA with a significantly thicker (150 µm) layer of SU-8 applied via spin-coating; however, this is difficult to compare to our results without being able to standardize for electrode area. Meanwhile, Cooper et al. show microamp levels of leakage with an electrode of area 12.6 cm^2, a six order of magnitude increase in leakage current for an electrode four orders of magnitude larger than ours[44]; yet, again, direct comparison is difficult due to the vastly different electrode size and deposition methods. While the dielectric constant of SU-8 is relatively low,[45] the ability to passivate against leakage current is associated more with the ability to exclude ions, and while proton diffusivity (a good proxy for ion diffusivity in general) can easily be found for oxides,[46] it does not seem to be studied as much for polymers.

Hard-Bake Time Analysis

In addition to the width of SU-8, previous reports have demonstrated improved passivation layer performance through the modification of other parameters. For example, soft-/hard-bake times and temperatures have been explored to achieve even films that have improved mechanical properties[47] and thus do not delaminate or crack.[48,49] A hard bake is an extended period of heating after exposure of a resist that is intended to increase the cross-link density of the polymer, and hard-bake time has been largely overlooked in investigations of resist-based passivation layers. Olziersky et al. demonstrated that hard-baking SU-8 increases its ability to passivate GaInZnO (GIZO) against air,[23] but they only investigated a 1-h hard bake at 160°C. To examine the effect of hard-bake time on ionic solution passivation, SU-8 films with the same width of ≈350 µm were printed and their ability to passivate electrodes was measured as a function of hard-bake time. We found that a hard-bake time of 15 min yielded the lowest leakage current, with leakage current increasing with any further time (Fig. 3a). These results indicate that the elevated temperature may have initiated some degradation in the polymeric structure that overwhelmed the passivation gains made from the increased cross-linking. Further investigation is required to examine the fundamental mechanism at the root of this degradation at longer hard-bake times. As before, we measured the degradation of passivation over time, and did not find a distinct difference between this set of samples, which varied the hard-bake time (Fig. 3c), and the previous set, which analyzed different widths.

Conclusion

Electronic biosensors frequently suffer from performance drift and degradation when exposed to biological fluids due to contact between electronic components and ions in the solution. SU-8 is commonly used to passivate electrodes against ionic solutions; however, it is currently patterned primarily with cleanroom techniques, which increases cost

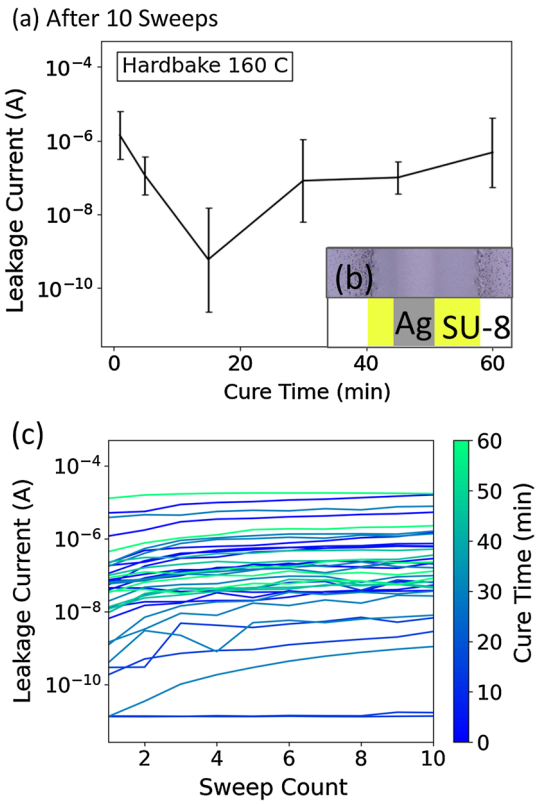

Fig. 3 Passivation dependence on hard-bake time. (a) Geometric average of 99.5th percentile of leakage plotted against cure time; error bars represent geometric standard deviation. Measured after 10 sweeps, leakage current is lowest for a hard-bake time of 15 min. Inset: (b) top-down diagram and photo of an example sample. (c) 99.5th percentile leakage current plotted against sweep count. Despite varying cure time, most chips show a similar increase in leakage current over time.

and complexity. We demonstrate that undiluted SU-8 can be aerosol-jet-printed to produce well-defined, continuous lines that can be used to passivate against PBS. It was found that the extent that the SU-8 extends beyond the electrode plays a key role in the quality of the passivation and an extension of around 100 µm on each side was found to be ideal for covering printed Ag electrodes. A hard-bake time of 15 min was determined to further improve the quality of the printed SU-8 passivation to an average peak leakage current of 1 nA at 0.5 V. Biosensors are frequently used for longitudinal measurement and thus temporal degradation was investigated. Printed SU-8 shows some degradation in passivation ability over time, although it is limited, with the majority being less than 25-fold. These findings demonstrate the ability to produce low-cost electronics for biosensing applications via the aerosol jet printing of both electronics and passivation layers.

Supplementary Information The online version contains supplementary material available at https://doi.org/10.1007/s11664-021-09396-4.

Funding This study was funded by the National Institutes of Health (NIH) under grant 1R01HL146849.

Conflict of interest The authors declare that they have no conflict of interest.

References

1. Statista, Size of The U.S. Point of Care Diagnostics and Testing Market from 2015 to 2022, by Product (in Billion U.S. Dollars), 2017.
2. P. Bonini, M. Plebani, F. Ceriotti, and F. Rubboli, Errors in laboratory medicine. *Clin. Chem.* 48, 691 (2002).
3. A. Pandey, Y. Gurbuz, V. Ozguz, J.H. Niazi, and A. Qureshi, Graphene-interfaced electrical biosensor for label-free and sensitive detection of foodborne pathogenic *E. Coli* O157:H7. *Biosens. Bioelectron.* 91, 225 (2017).
4. P. Bergveld, A critical evaluation of direct electrical protein detection methods. *Biosens. Bioelectron.* 6, 55 (1991).
5. L. Torsi, M. Magliulo, K. Manoli, and G. Palazzo, Organic field-effect transistor sensors: a tutorial review. *Chem. Soc. Rev* 42, 8612 (2013).
6. M. Kaisti, Detection principles of biological and chemical FET sensors. *Biosens. Bioelectron.* 2, 1098 (2019).
7. D. Sticker, M. Rothbauer, V. Charwat, J. Steinkühler, O. Bethge, E. Bertagnolli, H.D. Wanzenboeck, and P. Ertl, Zirconium dioxide nanolayer passivated impedimetric sensors for cell-based assays. *Sens. Actuators B Chem.* 213, 35 (2015).
8. W. Oelßner, J. Zosel, U. Guth, T. Pechstein, W. Babel, J.G. Connery, C. Demuth, M.G. Gansey, and J.B. Verburg, Encapsulation of ISFET sensor chips. *Sens. Actuators B Chem.* 105, 104 (2005).
9. P. Georgiou, and C. Toumazou, ISFET characteristics in CMOS and their application to weak inversion operation. *Sens. Actuators B Chem.* 143, 211 (2009).
10. W. Olthuis, A. Volanschi, J.G. Bomer, and P. Bergveld, A new probe for measuring electrolytic conductance. *Sens. Actuators B. Chem.* 13, 230 (1993).
11. F.R. Castiello, J. Porter, P. Modarres, and M. Tabrizian, Interfacial capacitance immunosensing using interdigitated electrodes: the effect of insulation/immobilization chemistry. *Phys. Chem. Chem. Phys.* 21, 15787 (2019).
12. C. Barrett, K. Dawson, C. O'Mahony, and A. O'Riordan, Development of low cost rapid fabrication of sharp polymer microneedles for in vivo glucose biosensing applications. *ECS J. Solid State Sci. Technol.* 4, S3053 (2015).
13. H. Zhang, S. Yang, and K. Sheng, The leakage mechanism of the package of the AlGaN/GaN liquid sensor. *Materials (Basel).* 13, 1903 (2020).
14. L. Li and A. J. Mason, Post-CMOS parylene packaging for on-chip biosensor arrays, in *Proceedings of IEEE Sensors* (2010), pp. 1613–1616.
15. P.A. Hammond, and D.R.G. Cumming, Encapsulation of a liquid-sensing microchip using SU-8 photoresist. *Microelectron. Eng.* 73–74, 893 (2004).
16. J. Gottschamel, L. Richter, A. Mak, C. Jungreuthmayer, G. Birnbaumer, M. Milnera, H. Brü, and P. Ertl, Development of a disposable microfluidic biochip for multiparameter cell population measurements. *Anal. Chem.* 81, 8503 (2009).
17. M.J. Milgrew, M.O. Riehle, and D.R.S. Cumming, A Large Transistor-Based Sensor Array Chip for Direct Extracellular Imaging, *Sensors and Actuators B Chemical*, Vol. 111. ed. F. Milgrew (London: Elsevier, 2005), pp. 347–353.
18. X. Xie, L. Rieth, S. Merugu, P. Tathireddy, and F. Solzbacher, Plasma-assisted atomic layer deposition of Al_2O_3 and parylene C Bi-layer encapsulation for chronic implantable electronics. *Appl. Phys. Lett.* 101, 093702 (2012).
19. G. Grau, and V. Subramanian, Dimensional scaling of high-speed printed organic transistors enabling high-frequency operation. *Flex. Print. Electron.* 5, 014013 (2020).
20. M.J. Milgrew, P.A. Hammond, and D.R.S. Cumming, The Development of Scalable Sensor Arrays Using Standard CMOS Technology, *Sensors and Actuators B Chemical*, Vol. 103. ed. J. Milgrew (London: Elsevier, 2004), pp. 37–42.
21. H. Lorenz, M. Despont, N. Fahrni, N. LaBianca, P. Renaud, and P. Vettiger, SU-8: a low-cost negative resist for MEMS. *J. Micromech. Microeng.* 7, 121 (1997).
22. K.V. Nemani, K.L. Moodie, J.B. Brennick, A. Su, and B. Gimi, In Vitro and in Vivo evaluation of SU-8 biocompatibility. *Mater. Sci. Eng. C* 33, 4453 (2013).
23. A. Olziersky, P. Barquinha, A. Vilà, L. Pereira, G. Gonçalves, E. Fortunato, R. Martins, and J.R. Morante, Insight on the SU-8 resist as passivation layer for transparent Ga_2O_3–In_2O_3–ZnO thin-film transistors. *J. Appl. Phys.* 108, 64505 (2010).
24. Z. Mao, K. Yoshida, and J.K. Wan, Fast packaging by a partially-crosslinked SU-8 adhesive tape for microfluidic sensors and actuators. *Sens. Actuators A Phys.* 289, 77 (2019).
25. A. Sadana, and N. Sadana, Market Size and Economics for Biosensors, *Fractal Analysis of the Binding and Dissociation Kinetics for Different Analytes on Biosensor Surfaces*. ed. J. Tarabella (London: Elsevier, 2008), pp. 317–334.
26. G. Tarabella, D. Vurro, S. Lai, P. D'Angelo, L. Ascari, and S. Iannotta, Aerosol jet printing of PEDOT: PSS for large area flexible electronics. *Flex. Print. Electron.* 5, 014005 (2020).
27. N.X. Williams, N. Watson, D.Y. Joh, A. Chilkoti, and A.D. Franklin, Aerosol jet printing of biological inks by ultrasonic delivery. *Biofabrication* 12, 025004 (2020).
28. N.J. Wilkinson, M.A.A. Smith, R.W. Kay, and R.A. Harris, A review of aerosol jet printing—a non-traditional hybrid process for micro-manufacturing. *Int. J. Adv. Manuf. Technol.* 105, 4599 (2019).
29. H. A. Gieser, D. Bonfert, H. Hengelmann, H. Wolf, K. Bock, V. Zollmer, C. Werner, G. Domann, J. Bahr, I. Ndip, B. Curran, F. Oehler, and H. Milosiu, in *Rapid Prototyping of Electronic*

Modules Combining Aerosol Printing and Ink Jet Printing, in Electronics System Integration Technology Conference, ESTC 2010-Proceedings (2010).
30. S. Agarwala, G. L. Goh, and W. Y. Yeong, Optimizing Aerosol Jet Printing Process of Silver Ink for Printed Electronics, in *IOP Conference Series: Materials Science and Engineering*, vol. 191 (Institute of Physics Publishing, 2017), p. 012027.
31. J.B. Andrews, J.A. Cardenas, C.J. Lim, S.G. Noyce, J. Mullett, and A.D. Franklin, Fully printed and flexible carbon nanotube transistors for pressure sensing in automobile tires. *IEEE Sens. J.* 18, 7875 (2018).
32. N.X. Williams, B. Carroll, S.G. Noyce, H.A. Hobbie, D.Y. Joh, J.G. Rogers, and A.D. Franklin, Fully printed prothrombin time sensor for point-of-care testing. *Biosens. Bioelectron.* 172, 112770 (2021).
33. G.L. Goh, S. Agarwala, Y.J. Tan, and W.Y. Yeong, A low cost and flexible carbon nanotube PH sensor fabricated using aerosol jet technology for live cell applications. *Sens. Actuators B Chem.* 260, 227 (2018).
34. K. Parate, S.V. Rangnekar, D. Jing, D.L. Mendivelso-Perez, S. Ding, E.B. Secor, E.A. Smith, J.M. Hostetter, M.C. Hersam, and J.C. Claussen, Aerosol-jet-printed graphene immunosensor for label-free cytokine monitoring in serum. *ACS Appl. Mater. Interfaces* 12, 8592 (2020).
35. MicroChem, SU-8 TF 6000, n.d.
36. M. Robin, W. Kuai, M. Amela-Cortes, S. Cordier, Y. Molard, T. Mohammed-Brahim, E. Jacques, and M. Harnois, Epoxy based ink as versatile material for inkjet-printed devices. *ACS Appl. Mater. Interfaces* 7, 21975 (2015).
37. V. Fakhfouri, N. Cantale, G. Mermoud, J. Y. Kim, D. Boiko, E. Charbon, A. Martinoli, and J. Brugger, Inkjet printing of SU-8 for polymer-based mems a case study for microlenses, in *Proceedings of the IEEE International Conference on Micro Electro Mechanical Systems (MEMS)* (2008), pp. 407–410.
38. R. Bernasconi, M.C. Angeli, F. Mantica, D. Carniani, and L. Magagnin, SU-8 inkjet patterning for microfabrication. *Polymer (Guildf).* 185, 1096 (2019).
39. R. Eckstein, M. Alt, T. Rödlmeier, P. Scharfer, U. Lemmer, and G. Hernandez-Sosa, Digitally printed dewetting patterns for self-organized microelectronics. *Adv. Mater.* 28, 7708 (2016).
40. J.I. Reyes-De-Corcuera, H.E. Olstad, and R. García-Torres, Stability and stabilization of enzyme biosensors: the key to successful application and commercialization. *Annu. Rev. Food Sci. Technol.* 9, 293 (2018).
41. N.X. Williams, S. Noyce, J.A. Cardenas, M. Catenacci, B.J. Wiley, and A.D. Franklin, Silver nanowire inks for direct-write electronic tattoo applications. *Nanoscale* 11, 14294 (2019).
42. A. M. N. Al-Mobin, R. Shankar, W. Cross, J. Kellar, K. W. Whites, and D. E. Anagnostou, Advances in Direct-Write Printing of RF-MEMS Using M3D, in *IEEE MTT-S International Microwave Symposium Digest* (Institute of Electrical and Electronics Engineers Inc., 2014).
43. F. Zhang, C. Tuck, R. Hague, Y. He, E. Saleh, Y. Li, C. Sturgess, and R. Wildman, Inkjet Printing of Polyimide Insulators for the 3D Printing of Dielectric Materials for Microelectronic Applications. *J. Appl. Polym. Sci.* 133, 59 (2016).
44. C. Cooper, K. Eldridge, M.H. Kim, H. Yoon, S.H. Choi, and K.D. Song, Parylene-C Passivation and Effects on Rectennas' Wireless Power Transfer Performance, *Nanosensors, Biosensors, and Info-Tech Sensors and Systems*, Vol. 9060. ed. V.K. Varadan (New York: SPIE, 2014), p. 90601A.
45. A. Ghannam, C. Viallon, D. Bourrier, and T. Parra, Dielectric microwave characterization of the SU-8 thick resin used in an above IC Process, 009 Eur. Microw. Conf. 1041 (2009).
46. S. Choi, I. Park, Z. Hao, H.Y.N. Holman, and A.P. Pisano, Quantitative studies of long-term stable, top-down fabricated silicon nanowire PH sensors. *Appl. Phys. A Mater. Sci. Process.* 107, 421 (2012).
47. T. Winterstein, M. Staab, C. Nakic, H.-J. Feige, J. Vogel, and H. Schlaak, SU-8 electrothermal actuators: optimization of fabrication and excitation for long-term use. *Micromachines* 5, 1310 (2014).
48. Y. Li, Challenges and issues of using polymers as structural materials in MEMS: a review. *J. Microelectromech. Syst.* 2, 1697 (2019).
49. S. Keller, G. Blagoi, M. Lillemose, D. Haefliger, and A. Boisen, Processing of thin SU-8 films. *J. Micromech. Microeng.* 18, 125020 (2008).